DEUTSCHES ELEKTRONEN-SYNCHROTRON DESY

DESY 73/46
October 1973

Separation of Clusters in the Reaction $\pi^+ p \to \pi^+\pi^+\pi^- p$ at 11.7 GeV/c

by

E. Bassler
Deutsches Elektronen-Synchrotron DESY, Hamburg

H. Nagel and W. D. Schlatter
II. Institut für Experimentalphysik der Universität Hamburg

2 HAMBURG 52 · NOTKESTIEG 1

Separation of Clusters in the Reaction $\pi^+ p \to \pi^+\pi^+\pi^- p$ at 11.7 GeV/c *)

by

E. Bassler

Deutsches Elektronen-Synchrotron DESY, Hamburg

H. Nagel and W.D. Schlatter

II. Institut für Experimentalphysik der Universität Hamburg

Abstract:

We present a Monte-Carlo selection method in the full 3N-5 dimensional kinematic space and apply it to the reaction $\pi^+ p \to \pi^+ p \pi^+ \pi^-$ at 11.7 GeV/c.

The method is tested by comparing the results with those from maximum likelihood fits and by applying it to a simulated experiment.

The quasi two body reactions could be separated and their cross sections correctly determined. The method is shown to reproduce the differential distributions, at least of the more important reactions, without bias.

---

*) Contribution presented at the IVth International Symposium on Multiparticle Hadrodynamics - Pavia - Italy

I) Introduction

For the analysis of a multibody final state such as $p\pi^+\pi^+\pi^-$ many techniques are available. The separation of different processes like $\Delta^{++}\rho^o$ or pA_2, which contribute to the same final state, becomes less difficult at higher center of mass energy.

A model-independent analysis should be based on a kinematic separation using a complete set of parameters for the description of the outgoing particles. The space of all parameters is not uniformly populated by the experimental events. The different processes more or less form separated clusters. The aim of the analysis is to separate these clusters by a statistical method and to get pure samples for the different reactions.

This was tried first by Pless et al. (1) by the so called "prism plot technique" with the 3 and 4 body final states in a π^+p experiment at 3.9 GeV/c.

In this paper we report on the separation of the quasi two body reactions of the $\pi^+p \to p\pi^+\pi^+\pi^-$ channel at 11.7 GeV/c incident momentum. In the prism plot procedure of Pless et al. (1) the probability for one event to come from a particular process, was approximated in a manner inappropriate for large statistic experiments. We therefore use a different method that gives us an easily calculated approximation to this probability. We then study whether or not our selection method introduced biases. We show that one can separate the quasi two body reactions and obtain the correct cross sections. Also the production and decay angular distributions are reproduced without bias. Both were proved by a Monte-Carlo simulation of the experiment.

II) Details of the Method.

In an experiment with N final state particles and an unpolarized beam, one needs 3N-5 parameters to describe the kinematic configuration at fixed energy. In order that the different processes, such as production of various resonances contributing to the specific final state, can be best separated by finding the corresponding clusters formed in the 3N-5 dimensional space, C_{3N-5}, a judicious choice of coordinates is necessary.

As is well know, in the Van Hove variables of the longitudinal phase space (2) the main production mechanisms, such as double resonance production and diffractive processes, appear roughly separated.

To the N-1 Van Hove variables we add the N-1 kinetic energies and N-3 transverse momenta.

Since for the different processes of interest the distributions in these 3N-5 variables are not known in detail, one first simulates each process with a fixed number of Monte-Carlo events, with the appropriate mass distribution and isotropic production and decay distributions. We calculate for the Monte-Carlo events the 3N-5 coordinates of the space C_{3N-5} in which the experimental processes are to be separated. The distributions of the 3N-5 parameters of the simulated processes cover the corresponding clusters of the experimental events. For each experimental event one then finds the proportion of simulated events within a neighbourhood of the event which come from a particular process. This proportion is a first approximation to the probability that the event came from that particular process.

A simple way to specify the "neighbourhood" of each experimental event is to divide the space C_{3N-5} into M^{3N-5} cubes. For each cube a "tag", consisting of the set of probabilities determined from the Monte-Carlo simulation, is assigned to every experimental event in the cube; in other words, the event is distributed among the different processes according to this probability.

In a second iteration the Monte-Carlo events are generated with production and decay angular distributions as were found for the tagged events for each of the processes. New tags are then computed.

The generation of Monte-Carlo events with better angular distributions and the tagging of the experimental events is continued until the distributions of the tagged events do not change from one iteration to the next.

III) Investigation of the $\pi^+ p \pi^+ \pi^-$-Channel

III.1) Variables

With the procedure explained above for separating clusters we analysed the 4 body final state $p\pi^+\pi^+\pi^-$ of the $\pi^+ p$ bubble chamber experiment at 11.7 GeV/c incident momentum, performed with the 2m HBC at CERN. For our analysis we used 9471 $\pi^+ p \to p\pi^+\pi^+\pi^-$ events corresponding to a cross section of (1.45 ± 0.15) mb.

In the following we will discuss the 7 variables of C_7 for the 9471 $p\pi^+\pi^+\pi^-$ events.

The distribution of the two spherical angles Θ_1 and Θ_2 of the longitudinal momentum phase space (= Van Hove angles) is not uniform (see fig. 1). The lines with longitudinal momentum zero divide the $\Theta_1 - \Theta_2$-plane in different sectors. Most of the events lie in sectors with three different configurations of longitudinal momenta; these configurations correspond to double resonance, A-meson and isobar production.

The third Van Hove variable, the relative radius of the tetrahedron of longitudinal momenta, R/R_{max}, measures how peripheral the outgoing particles are. At $R = R_{max}$ all transverse momenta are zero. Fig. 2 shows the R/R_{max} distribution for all events, with the maximum at 0.96, and for $\Delta^{++}\rho^0$-events, with the maximum at 0.98. One clearly sees the peripheral character of the $\pi^+ p$ reactions at 11.7 GeV/c. Since pure phase space events should have a symmetric R/R_{max} distribution, one gets from the 40 events with $R/R_{max} < 0.5$ an upper limit of about 14 μb for the cross section of phase-space distributed events.

Another three variables are the coordinates of the simplex of kinetic energies. Each event corresponds to a point within a tetrahedron, where the distances from the surfaces are the kinetic energies. The population of the tetrahedron shows some favoured regions within the kinematic limits (see fig.3).

To complete the set of variables we use the transverse momentum squared of the $\pi^+\pi^+$ combination.

III.2) Test of the Method

To get confidence that the above method will not introduce significant biases in the differential distributions of the various processes of the final state $\pi^+ p \pi^+ \pi^-$ we simulated the experimental input by Monte-Carlo events.

From our previous studies (3), (4), (5) we know that the following processes are strong contributors to the final state $\pi^+ p \pi^+ \pi^-$:

1) $\pi^+ p \to \Delta^{++}(1236)\ \rho^o$

2) $\pi^+ p \to \Delta^{++}(1236)\ f$

3) $\pi^+ p \to \Delta^{++}(1236)\ g$

4) $\pi^+ p \to \Delta^{++}(1950)\ \rho^o$

5) $\pi^+ p \to \Delta^{++}(1236)\ \pi^+\pi^-$

6) $\pi^+ p \to p\pi^+\ \rho^o$

7) $\pi^+ p \to A_1 p \to \rho^o \pi^+ p$

8) $\pi^+ p \to A_2 p \to \rho^o \pi^+ p$

9) $\pi^+ p \to A_3 p \to f\pi^+ p$

For the model experiment we simulated processes 1) - 4), 7) and 9) according to the known production and decay behaviour, and we left out the remaining three processes. The four momentum transfer squared, t, to the resonances was limited to $|t| < 1.5$ GeV $(\text{GeV/c})^2$ and the resonance mass distribution to $M = M_o \pm 500$ MeV.

Analysing then our selection method, the cross sections were found correctly within 5 - 10 %. As expected, almost no events were tagged for processes 5), 6) and 8).

We compared the production and decay angular distributions found with our selection method, with the Monte-Carlo input. The systematic deviations as measured by the Kolmogorov-Smirnov statistic (6) were found to be small, compared with the statistical errors of our actual experiment. Thus, our procedure is superior to applying simple longitudinal momentum cuts which are known to influence the angular distributions. In our case, the 7 dimensional clusters corresponding to the separate processes, are separated by functions which depend on all 7 variables instead of momentum cuts that depend on only one variable.

III.3 Production Cross Sections

As described in the above section we choose the reactions 1) - 9) for the analysis of the $p\pi^+\pi^+\pi^-$ final state. We find that the effective mass distributions of the resonances of the tagged events for processes 1) - 6) are well described

by pure Breit-Wigner functions without any background. The events in the histograms are weighted with the probability for each event to contribute to the particular process (see fig. 4 for processes 1) - 3)). The π^+ of the pion-pion resonance is denoted π_1^+, the other by π_2^+. In the case of Δ^{++} the π_2^+ has the higher four momentum transfer squared, $t = |(p(\pi^+_{in}) - p(\pi^+_{out}))^2|$.

Due to the simplicity of our tagging method, there is still some ρ^o in the $\pi_1^+\pi^-$ mass distribution of the "Δ^{++}f" channel. But with two Breit-Wigner functions for the ρ^o and the f the $\pi_1^+\pi^-$ mass spectrum is well described. Similarly, there is f contamination in the "Δ^{++}g" cluster. To get rid of these wrongly assigned events the ρ^o mass is limited to $M(\pi_1^+\pi^-) < 1.05$ GeV, the f to $1.05 \text{ GeV} < M(\pi_1^+\pi^-) < 1.50$ GeV and the g to $1.50 \text{ GeV} < M(\pi_1^+\pi^-)$. The effective masses $M(p\pi_2^+)$ and $M(\pi^+\pi^+\pi^-)$ in Fig. 4 are for these $\pi_1^+\pi^-$ mass bands.

In the case of the A mesons there remained some background under the ρ^o, A_1 and A_2 for the tagged events. These distributions were fitted with a third degree polynomial background (fig. 5 for reaction 7) - 9)). The A_1 and A_3 were not described by Breit-Wigner functions because it appears from phase shift results (7) that these effects are not Breit-Wigner resonances.

The total cross sections for the processes 1) - 9) were determined from the numbers of tagged events, with the Breit-Wigner fits used to correct for the occurence of some ρ^o in the f sample, and f in the g sample. It is not possible to calculate the errors on the cross sections obtained with the cluster separation. We can only estimate the errors by observing the fluctuations of the cross section when some technical details are changed, such as the bin size of the cubes of C_7.

In table 1 the cross sections found for reactions 1) - 9) are listed.

Table 1.

	reaction	cross section (μb)
1	$\pi^+p \to \Delta^{++}(1236)\ \rho^o$	290 ± 36
2	$\pi^+p \to \Delta^{++}(1236)$ f	110 ± 24
3	$\pi^+p \to \Delta^{++}(1236)$ g	35 ± 7
4	$\pi^+p \to \Delta^{++}(1950)\ \rho^o$	24 ± 6
5	$\pi^+p \to \Delta^{++}(1236)\ \pi^+\pi^-$	80 ± 13
6	$\pi^+p \to p\pi^+\ \rho^o$	$\leq$ 10
7	$\pi^+p \to pA_1$	105 ± 15
8	$\pi^+p \to pA_2$	55 ± 9
9	$\pi^+p \to pA_3$	65 ± 10

The $\Delta^{++}\rho^{o}$ and $\Delta^{++}f$ cross sections had been determined earlier with a maximum likelihood fit (3), (4). The results $\sigma(\Delta^{++}\rho) = (320 \pm 40)$ µb and $\sigma(\Delta^{++}f) = (110 \pm 15)$ µb from this fit agree very well with those from the cluster separation.

To study the differential cross sections of processes 1) - 9) we limited the effective masses of the $\pi_1^+\pi^-$ resonances to the bands defined above. The $\Delta^{++}(1236)$ is limited to $M(p\pi_2^+) < 1.5$ GeV in order to be consistent with observations of the resonance shape from π^+p phase shift analysis (8). The $d\sigma/dt$ distributions are shown in fig. 6. To compare the overall behaviour of $d\sigma/dt$ we fitted exponentials $e^{-a|t|}$ to it; a varies from 1.0 $(GeV/c)^{-2}$ to 20.0 $(GeV/c)^{-2}$.

In table 2 we give the different values for a.

Table 2. Slopes of $d\sigma/dt$

	a $(GeV/c)^{-2}$	t range for the fit $(GeV/c)^2$
$\Delta^{++}(1236)$ ρ^{o}	19.5 ± 1.0	.02 - .16
$\Delta^{++}(1236)$ f	12.0 ± 1.0	.08 - .32
$\Delta^{++}(1236)$ g	5.0 ± 0.6	.08 - .80
$\Delta^{++}(1950)$ ρ^{o}	7.0 ± 0.7	.10 - .60
$\Delta^{++}(1236)$ $\pi^+\pi^-$	1.4 ± 0.1	.10 - 1.6
$p\pi^+\pi^{o}$	1.3 ± 0.1	.20 - 1.6
pA_1	11.0 ± 0.5	.02 - .40
pA_2	7.1 ± 0.4	.02 - .40
pA_3	6.0 ± 0.5	.02 - .40

The absolute prediction of the one pion exchange model (OPE) agrees very well with the differential cross section of $\Delta^{++}\rho^{o}$ and $\Delta^{++}f$ (fig. 7). The result of our earlier determination (4) of $d\sigma/dt$ with the maximum likelihood fit in t bins, agrees with the present result for $\Delta^{++}\rho^{o}$ up to $|t| \sim 0.25$ $(GeV/c)^2$ (see fig. 7, the dotted lines give the upper and lower error limits of the maximum likelihood fit of ref. (3),(4)).

We conclude from these results that with the cluster separation one is able to select distinct processes. From the comparison of total and differential cross sections of $\Delta^{++}\rho^{o}$ and $\Delta^{++}f$ with the result of the maximum likelihood fit and the OPE model we see that no systematic loss is caused by the cluster separation.

Within the selected clusters we do not observe processes other than 1) - 9). About 2770 events had no Monte Carlo events in their cube after the last interation.

From mass plots (not shown) of these untagged events, we found that most were from production of higher isobars.

III.4 Decay Distributions.

We measure the decay angles of the resonances in the Gottfried-Jackson frame (z axis: incoming particle; y axis: production normal; both in the resonance rest frame).

The polar angle distribution of $\Delta^{++}\rho^{o}$ and $\Delta^{++}f$ for the tagged events are presented in fig. 8. We can compare the $\cos\Theta$ distribution of the events obtained with cluster separation, with fits of the theoretical angular function to all events inside the double-resonance regions. The asymmetry in the case of $\Delta^{++}\rho^{o}$ comes from the known S-P wave interference which we took into account by adding the spherical harmonics Y_1^o and Y_1^1 to the angular function.

For the f meson sample some asymmetry in $dN/d\cos\Theta$ is observed. A similar asymmetry has already been observed in the decay distribution for the double-resonance region at this energy and at 13.1 GeV/c (8).

From the expansion of the normalized angular distribution $dW/d\cos\Theta$ in Legendre polynomials one can learn about interferences and polarisation of the $\pi^+\pi^-$ system. We have

$$dW/d\cos\Theta = \sum_{l=0}^{\infty} a_l P_l(\cos\Theta) \text{ with } \frac{2}{2l+1} a_l = \langle P_l(\cos\Theta)\rangle = \frac{1}{N} \sum P_l(\cos\Theta)$$

The expansion coefficients for the processes 1), 2), 3) with the polar angle Θ measured in the Gottfried-Jackson frame are shown in fig. 9. $\langle P_l\rangle$ for $\pi_1^+\pi^-$ events in the $\Delta^{++}\rho^{o}$ cluster shows S-P wave interference, presumably from the

$\varepsilon(700)$. The f meson from the Δ^{++}f cluster is indicated by a bump in $\langle P_4 \rangle$. ρ-f interference in the f mass region can explain the structure of $\langle P_1 \rangle$ and $\langle P_3 \rangle$ for the Δ^{++}f cluster. The vanishing of $\langle P_1 \rangle$ with $l \geq 5$ indicates that there are no further interferences in the Δ^{++}f cluster.

The broad g peak ($\Gamma \approx 170$ MeV) for the Δ^{++}g cluster is seen only in $\langle P_2 \rangle$ and $\langle P_4 \rangle$. The rather flat distribution of $\langle P_6 \rangle$ could be caused by a lack of polarisation of the g meson. But we cannot exclude that our method of dividing the space C_7 in cubes, is too coarse for a small statistic process like Δ^{++}g, and that therefore the dN/dcosΘ distribution may not have been correctly obtained.

The expansion in Legendre polynomials for the A meson decays uses the polar angle of the normal $\pi_1^+ \times \pi_2^+$ in the three pion rest frame. The $A_1 \to \rho\pi$ cluster is clearly dominated by the P wave ($\langle P_2 \rangle$ in fig. 10). The $A_2 \to \rho\pi$ decay with $J^P = 2^+$ is reflected in $\langle P_4 \rangle$ for the events in the A_2 cluster. At the mass $M(\pi^+\pi^+\pi^-) \approx 1640$ MeV for the $A_3 \to f\pi$ cluster, only $\langle P_2 \rangle$ shows a clear maximum. The contribution to $\langle P_4 \rangle$ of the A_3 is not very significant.

The moments with odd l values are all compatible with zero for the A_1, A_2 and A_3 clusters. This fact indicates that there are no dominant interferences in the three clusters.

IV. Conclusion.

We have shown that the many peripheral processes that contribute to the reaction $\pi^+p \to p\pi^+\pi^+\pi^-$ at 11.7 GeV/c, can be separated by a simple method that allows to investigate the distributions in all 7 independent kinematic variables. That this was possible is certainly due to the dominance of quasi two body reactions which form rather well-separated clusters in the kinematic space. The main processes like $\Delta^{++}(1236)\rho^o$, $\Delta^{++}(1236)$f, pA_1, pA_2 and pA_3 could be selected without bias in the angular distributions. Even reactions with quite small cross sections like Δ^{++}g and $\Delta^{++}(1950)\rho^o$ could be separated, although our simple method of cluster separation by dividing the total phase space in cubes probably causes some bias in the decay angular distributions of these small statistic processes.

Reactions not present in the experiment will not turn up spuriously due to our selection method; this was proved using a Monte-Carlo simulated experiment.

There were some events that could not be assigned to any of the processes considered in the selection procedure. In these we observe the production of heavior nucleon isobars, processes not considered in our procedure.

References.

1) F.T. Dao. M.F. Hodous, I.A. Pless; R.A. Singer,
PEPR-Programming Note MIT, Physics 101 (1971) and
J.E. Brau, F.T. Dao, M.F. Hodous, I.A. Pless and R.A. Singer,
Phys. Rev. Letters 21, 1481 (1971).

2) L. van Hove, Nucl. Phys. B9, 331 (1969).

3) Maddock et al., Nuovo Cimento A5, 433 (1971).

4) H. Nagel, DESY F1-71/7, Internal report, (Thesis).

5) C. Caso et al., Nucl. Phys. B36, 349 (1972).

6) B.W. Lindgren, "Statistical Theory", Macmillan, New York (1968).

7) G. Ascoli, Batavia Conference (1972) paper 442.

8) C. Quigg, F. v. Hippel, Argonne, ANL-HEP 7129 (1971).

9) J.A. Gaidos et al., Nucl. Phys. B26, 225 (1971).

Figure Captions.

Fig. 1. Van Hove angles Θ_1 versus Θ_2 for 9471 $\pi^+p\pi^+\pi^-$ events. The curves correspond to the longitudinal momentum q = 0 for each particle.

Fig. 2. Normalized radius R/R_{max} of the polyhedron of longitudinal momenta for all 9471 events. The hatched histogram shows the $\Delta^{++}\rho^o$ events. Dotted line for phase space is in arbitrary units.

Fig. 3. $\pi^+p\pi^+\pi^-$ events in the kinematic energy representation. The tetrahedron is shown from three views.

Fig. 4. Effective mass distributions obtained for the $\Delta^{++}\rho^o$, $\Delta^{++}f$ and $\Delta^{++}g$ clusters. The $M(\pi^+_2p)$ and $M(\pi^+\pi^+\pi^-)$ distributions are shown for the corresponding mass bands $M(\rho) < 1.05$ GeV $< M(f) < 1.50$ GeV $< M(g)$. The full lines are the fitted Breit-Wigner functions.

Fig. 5. Effective mass distributions obtained for the $A_1 \to \rho\pi$, $A_2 \to \rho\pi$ and $A_3 \to f\pi$ clusters. The $M(\pi^+_2p)$ and $M(\pi^+\pi^+\pi^-)$ distributions are shown for the corresponding ρ and f mass bands (see fig. 4). The curves are the fitted Breit-Wigner functions and the assumed background.

Fig. 6. Differential cross section of the tagged events for the reactions $\Delta^{++}(1236)\rho^o$, $\Delta^{++}(1236)f$, $\Delta^{++}(1236)g$, $\Delta^{++}(1236)\pi^+\pi^-$, $\Delta^{++}(1950)\rho^o$, $p\pi^+\rho^o$, pA_1, pA_2 and pA_3. The full line is the fitted function $A * e^{-a|t|}$ (values for a see table 2).

Fig. 7. Differential cross section of $\Delta^{++}\rho^o$ and $\Delta^{++}f$ compared with the absolute prediction of the OPE model and maximum likelihood fits from reference 3) and 4). (the dotted lines are the limits of one standard deviation).

Fig. 8. Angular distribution of $\Delta^{++}\rho^o$ and $\Delta^{++}f$ in the Gottfried-Jackson frame for the tagged events. The full lines are angular functions fitted to the double resonance regions.

Fig. 9. Legendre moments of the $\pi^+\pi^-$ polar angle distribution for the $\Delta^{++}\rho^o$ $\Delta^{++}f$ and $\Delta^{++}g$ clusters. The polar angle is measured in the Gottfried-Jackson frame.

Fig. 10. Legendre moments of the distribution of the normal to the three-pion decay plane, for the $A_1 \to \rho^o\pi$, $A_2 \to \rho\pi$, and $A_3 \to f\pi$ clusters. The polar angle of the decay normal is measured in the Gottfried-Jackson frame.

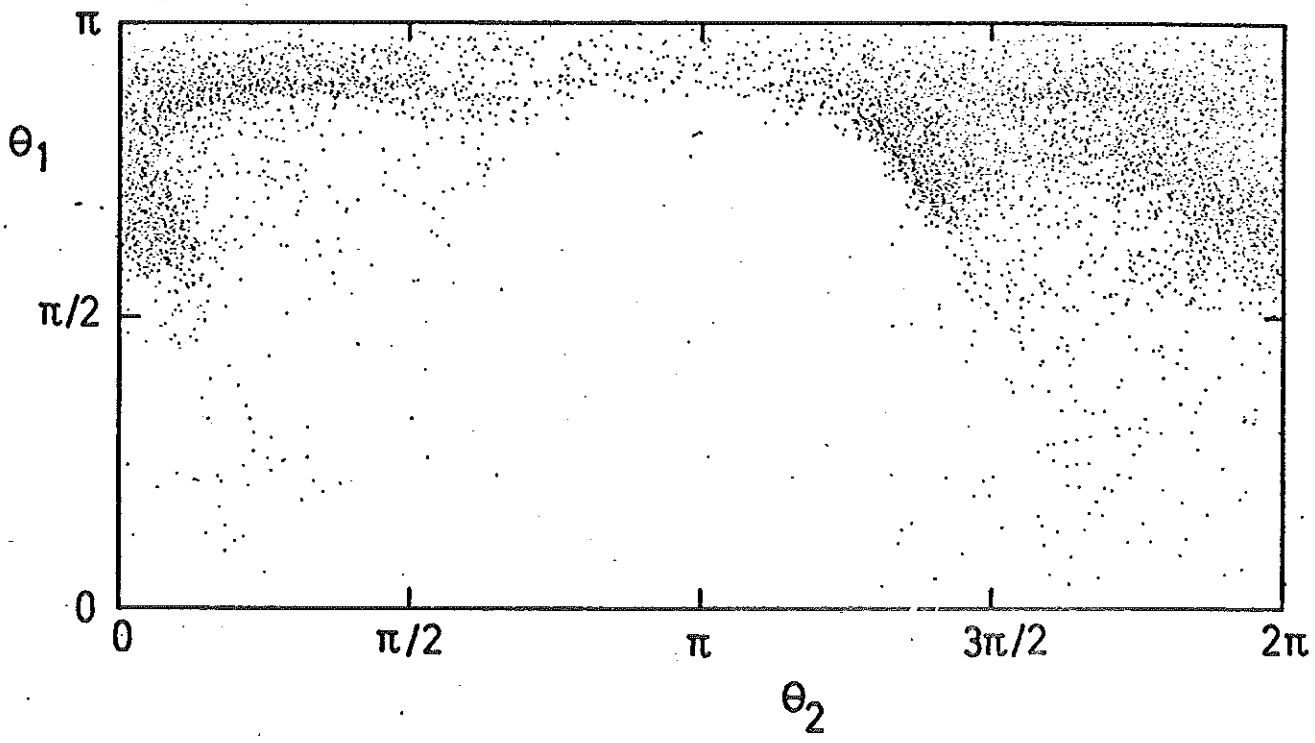

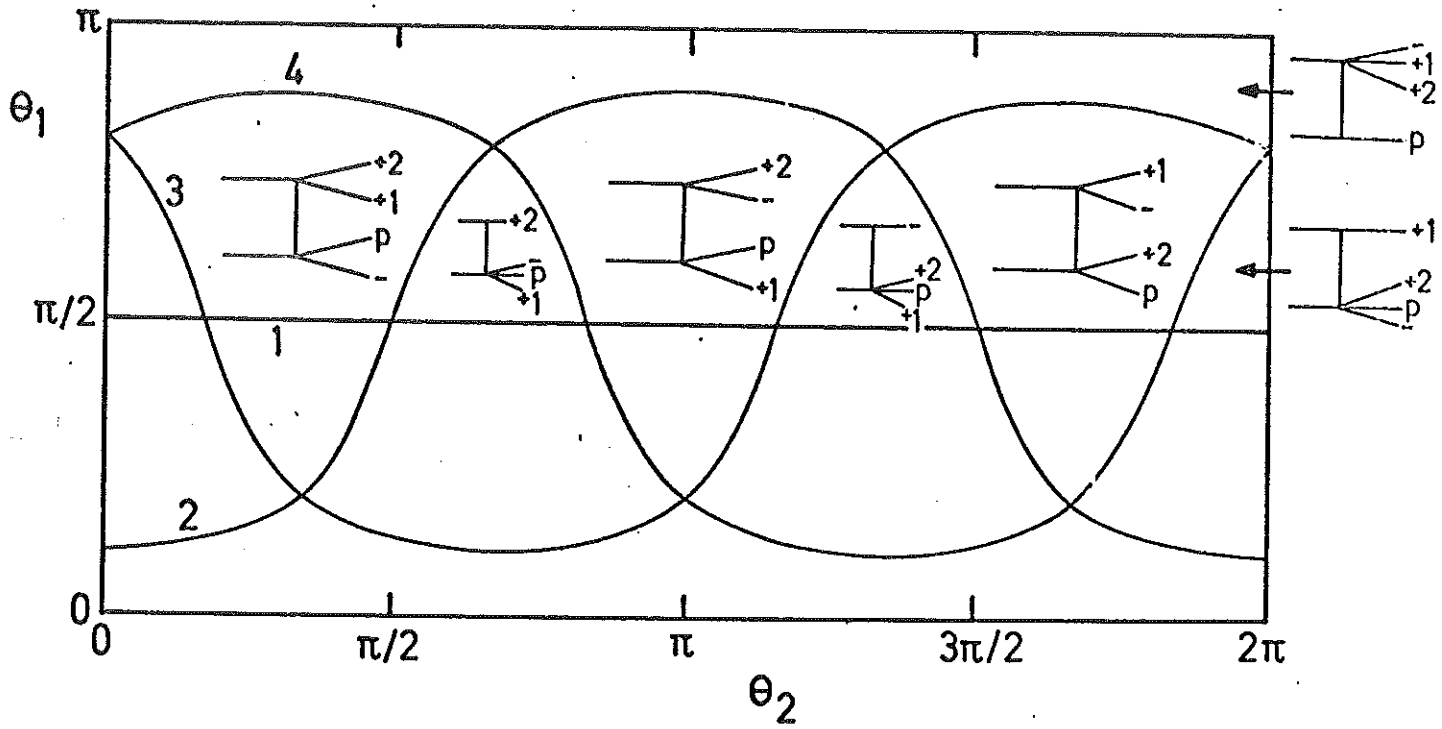

1) $q(p)=0$ 3) $q(\pi^+_2)=0$

2) $q(\pi^+_1)=0$ 4) $q(\pi^-)=0$

Fig.1

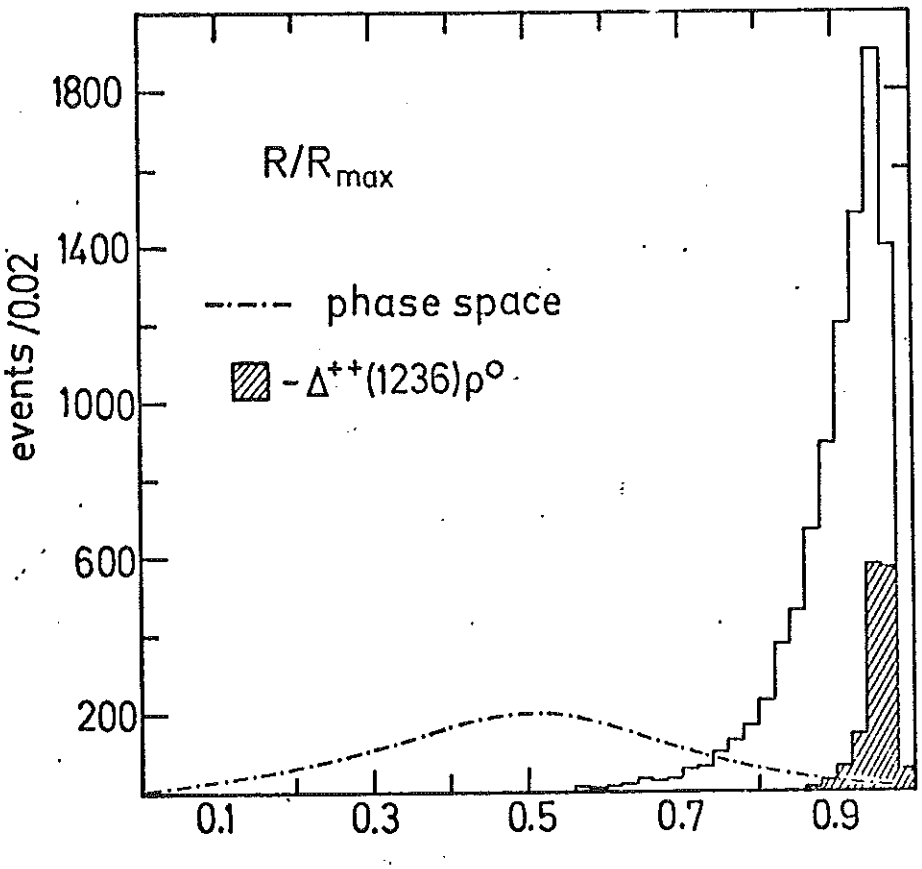
1800
1400
1000
600
200
events /0.02
R/R max
phase space
- Δ++(1236)ρ°
0.1
0.3
0.5
0.7
0.9

Fig.2

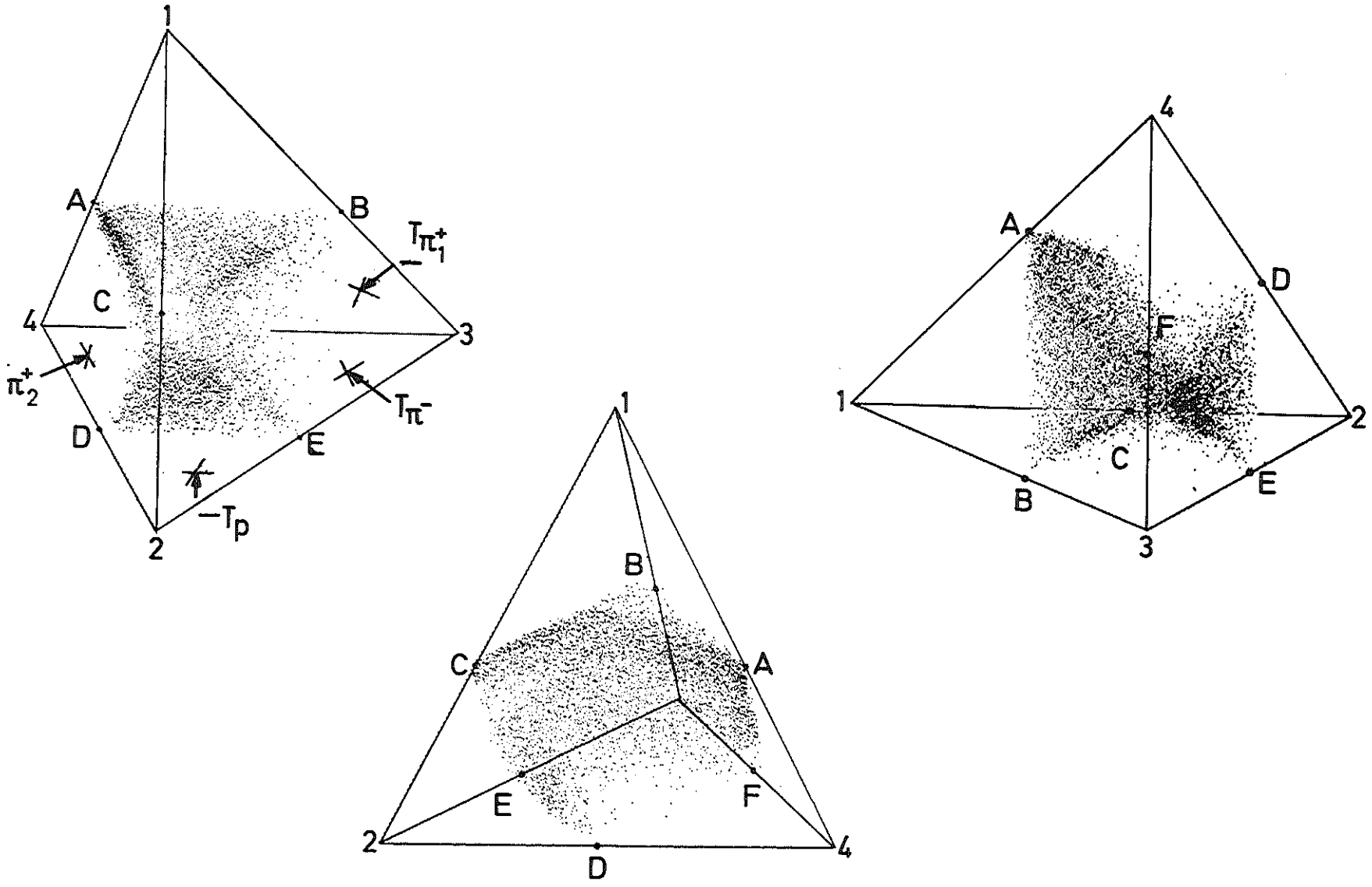

Fig.3

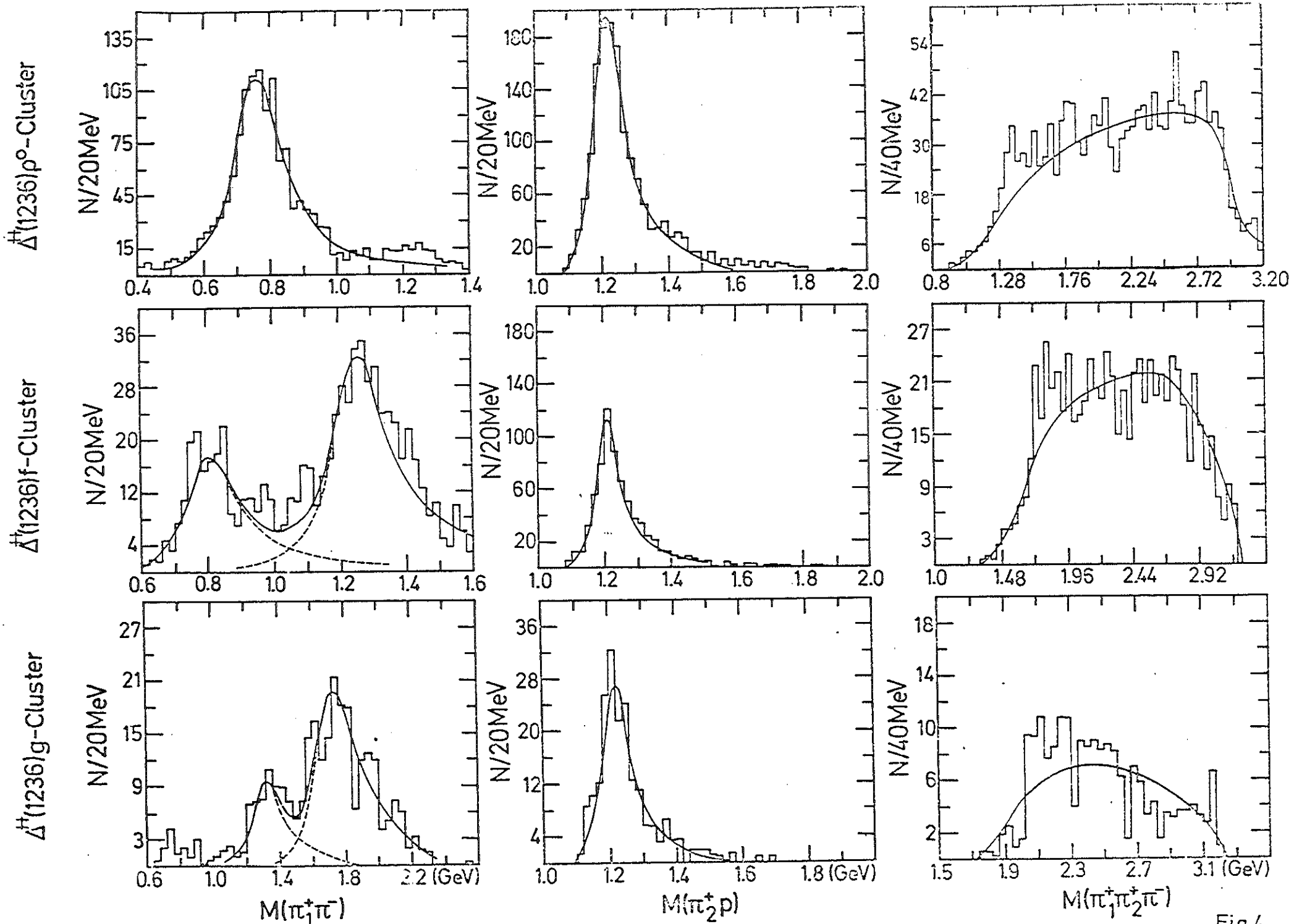
Δ++(1236)ρ°-Cluster
Δ++(1236)f-Cluster
Δ++(1236)g-Cluster
N/20MeV
N/40MeV
M(π1+π−)
M(π2+p)
M(π1+π2+π−)
(GeV)

Fig.4

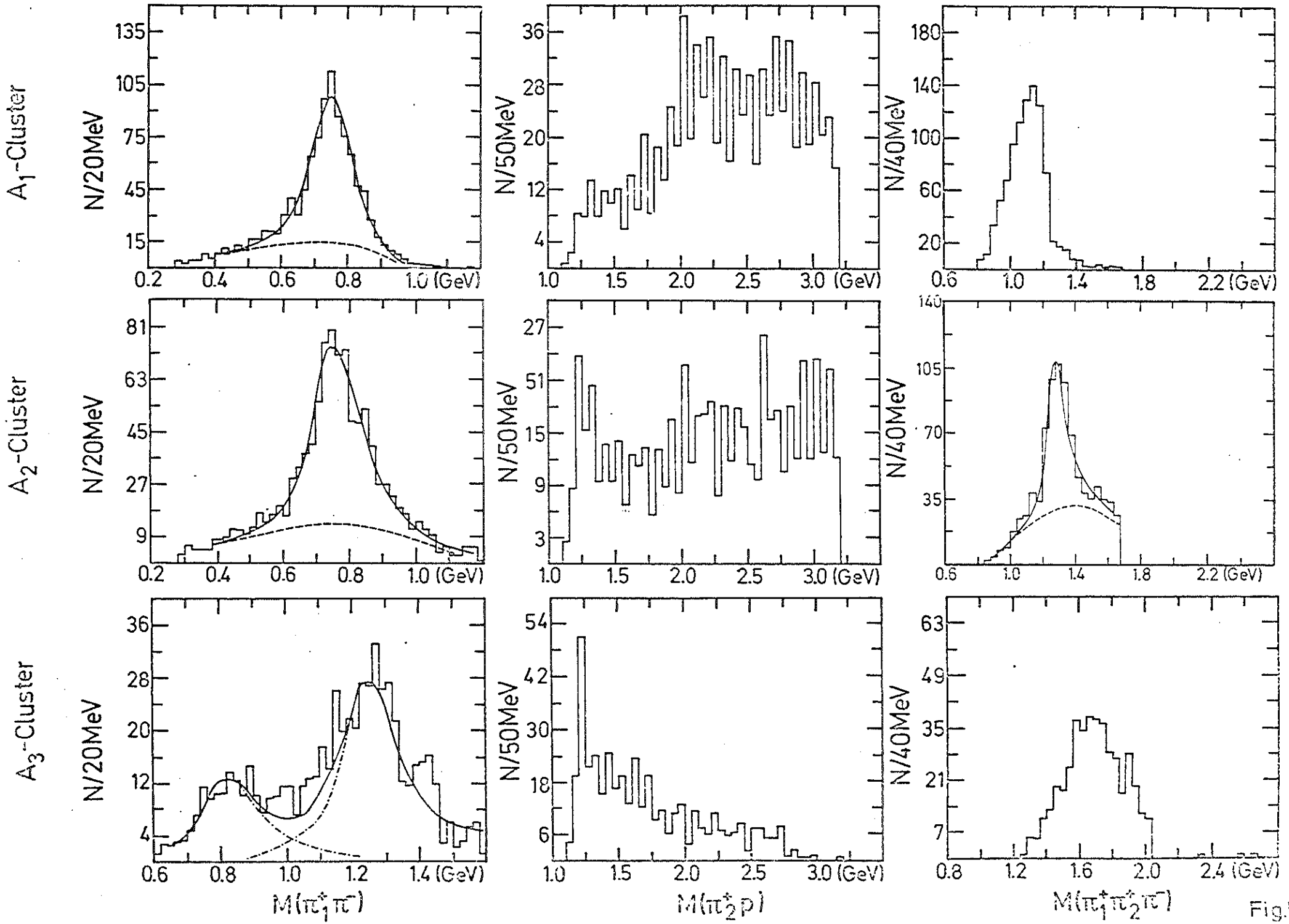
A1-Cluster
A2-Cluster
A3-Cluster
N/20MeV
N/50MeV
N/40MeV
M(π1+π−)
M(π2+p)
M(π1+π2+π−)
(GeV)

Fig.5

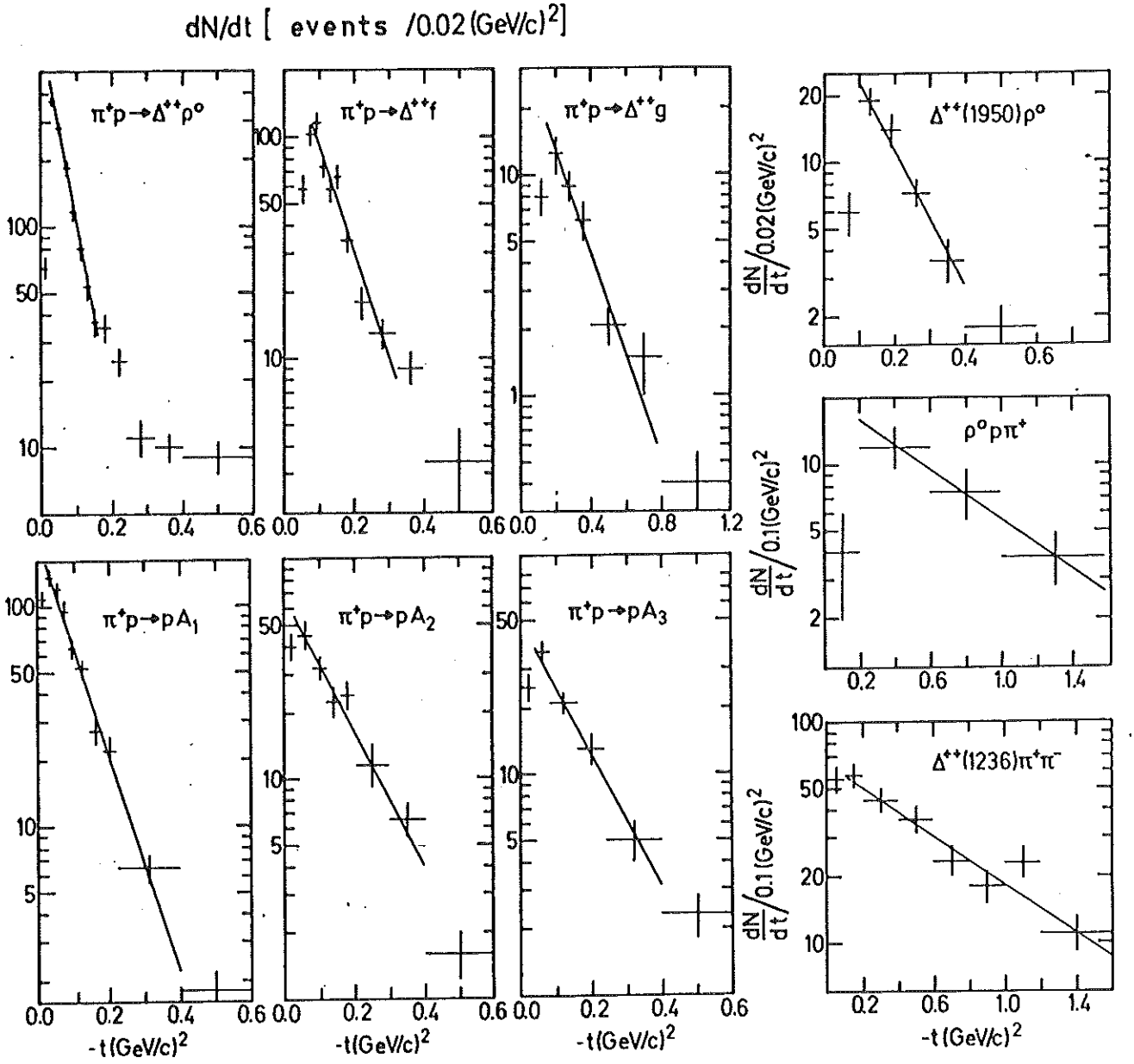
dN/dt [events /0.02 (GeV/c)²]
π⁺p→Δ⁺⁺ρ°
π⁺p→Δ⁺⁺f
π⁺p→Δ⁺⁺g
Δ⁺⁺(1950)ρ°
ρ°pπ⁺
Δ⁺⁺(1236)π⁺π⁻
π⁺p→pA₁
π⁺p→pA₂
π⁺p→pA₃
dN/dt /0.02 (GeV/c)²
dN/dt /0.1 (GeV/c)²
dN/dt /0.1 (GeV/c)²
-t (GeV/c)²
-t (GeV/c)²
-t (GeV/c)²
-t (GeV/c)²

Fig. 6

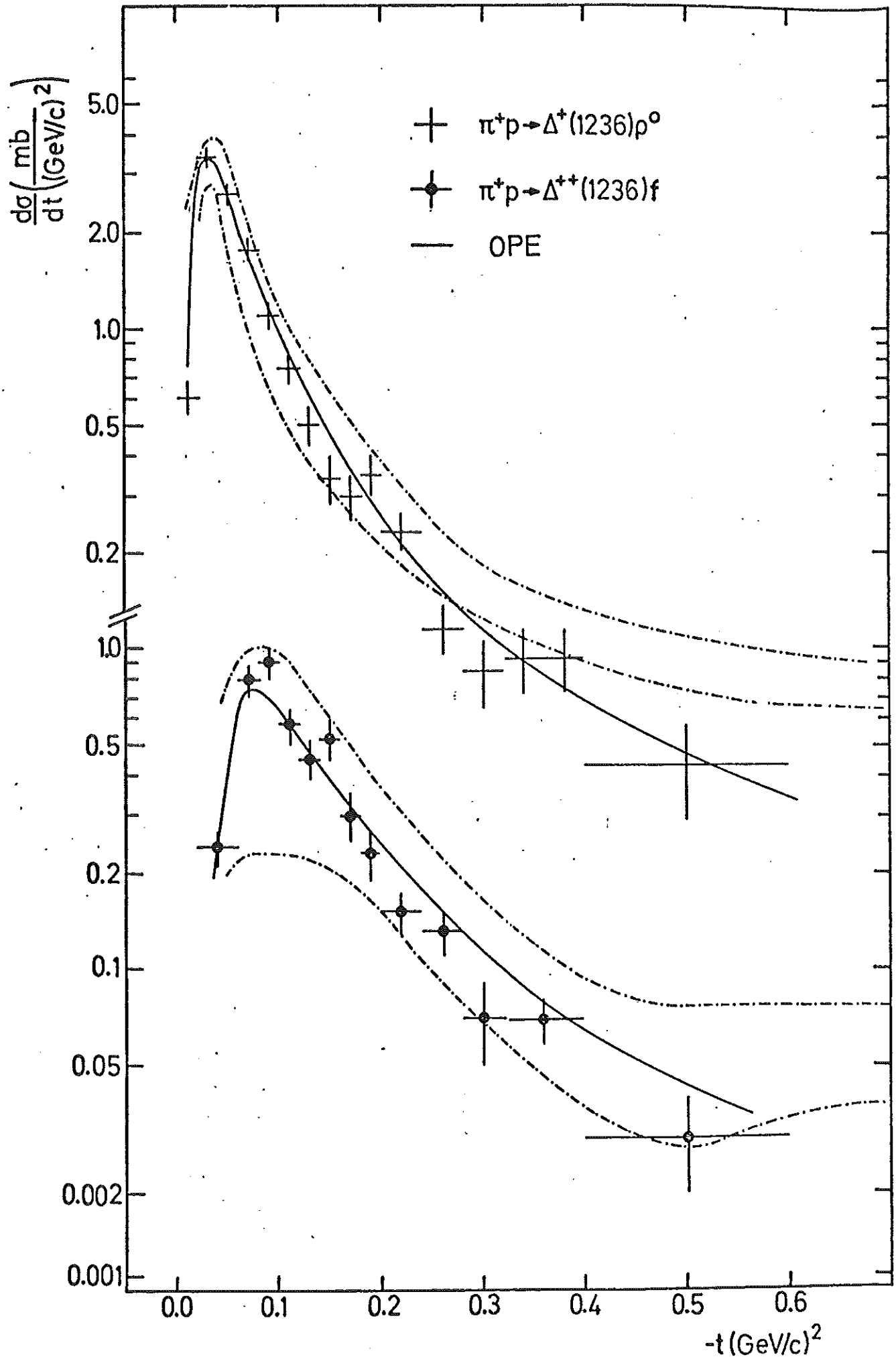
$\frac{d\sigma}{dt}\left(\frac{mb}{(GeV/c)^2}\right)$
$\pi^+p \to \Delta^+(1236)\rho^0$
$\pi^+p \to \Delta^{++}(1236)f$
OPE
5.0
2.0
1.0
0.5
0.2
1.0
0.5
0.2
0.1
0.05
0.002
0.001
0.0
0.1
0.2
0.3
0.4
0.5
0.6
$-t\,(GeV/c)^2$

Fig.7

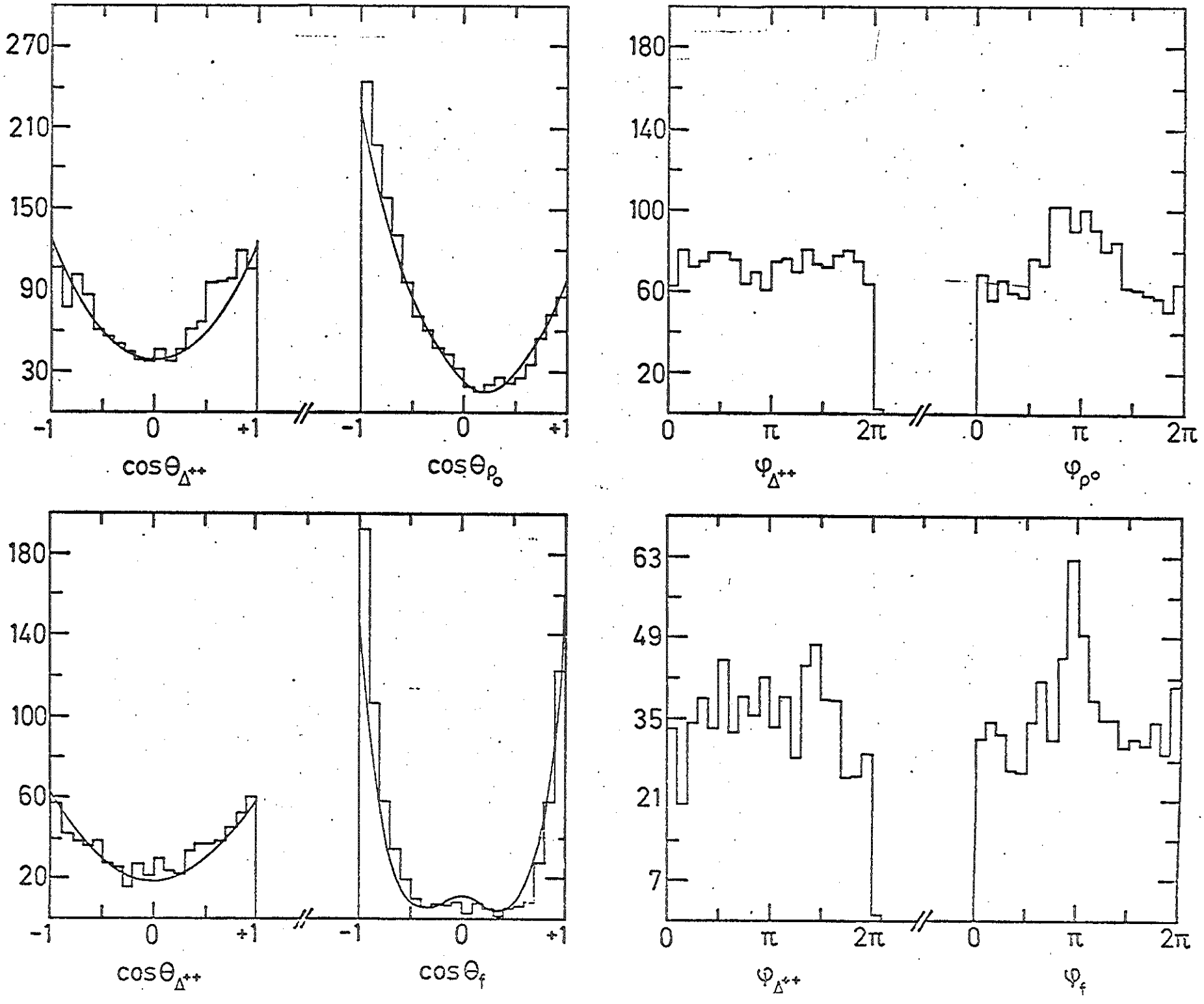
270
210
150
90
30
-1
0
+1
$\cos\theta_{\Delta^{++}}$
$\cos\theta_{\rho_0}$
180
140
100
60
20
0
π
2π
$\varphi_{\Delta^{++}}$
φ_{ρ^0}
63
49
35
21
7
$\cos\theta_{\Delta^{++}}$
$\cos\theta_f$
$\varphi_{\Delta^{++}}$
φ_f

Fig. 8

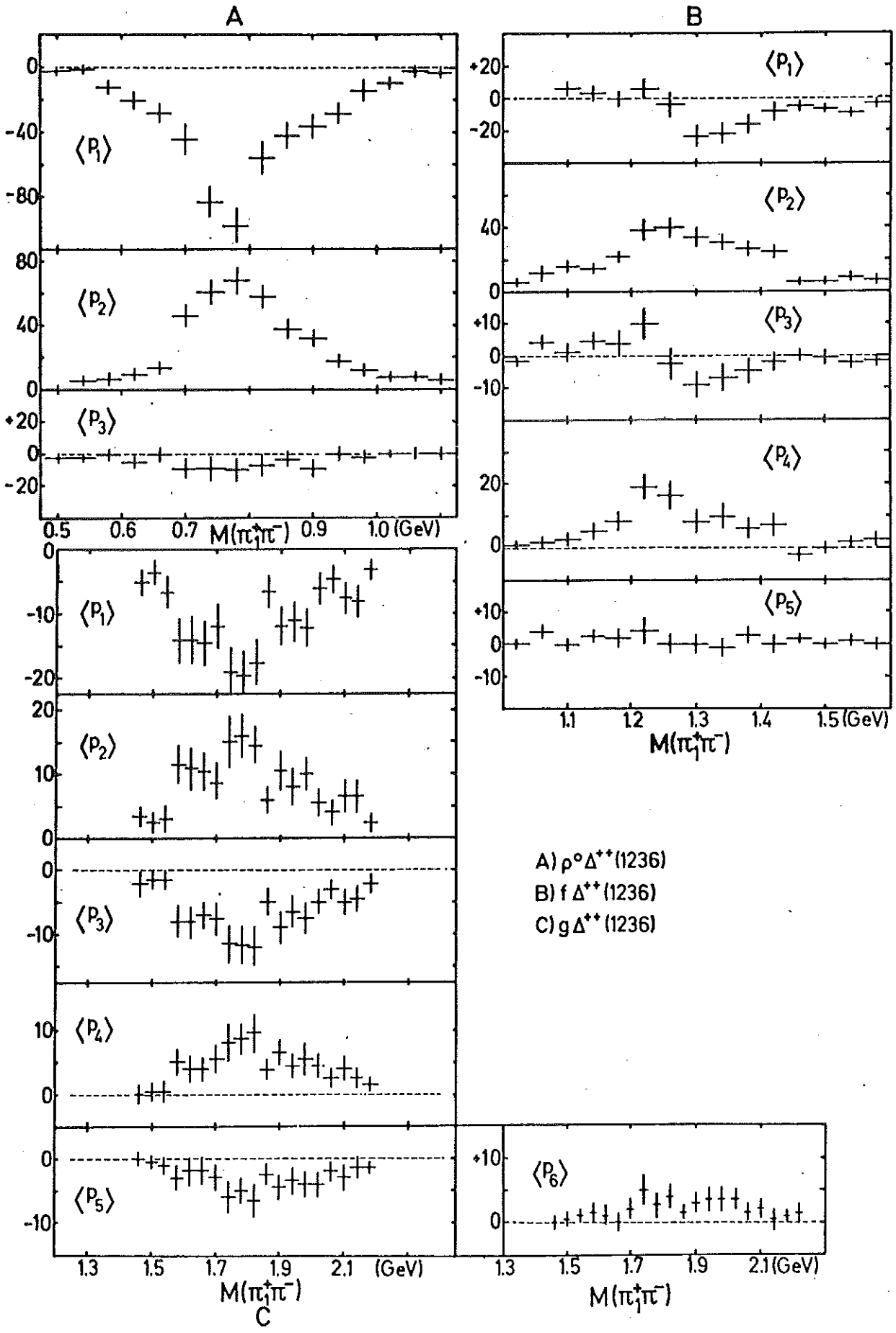

Fig.9

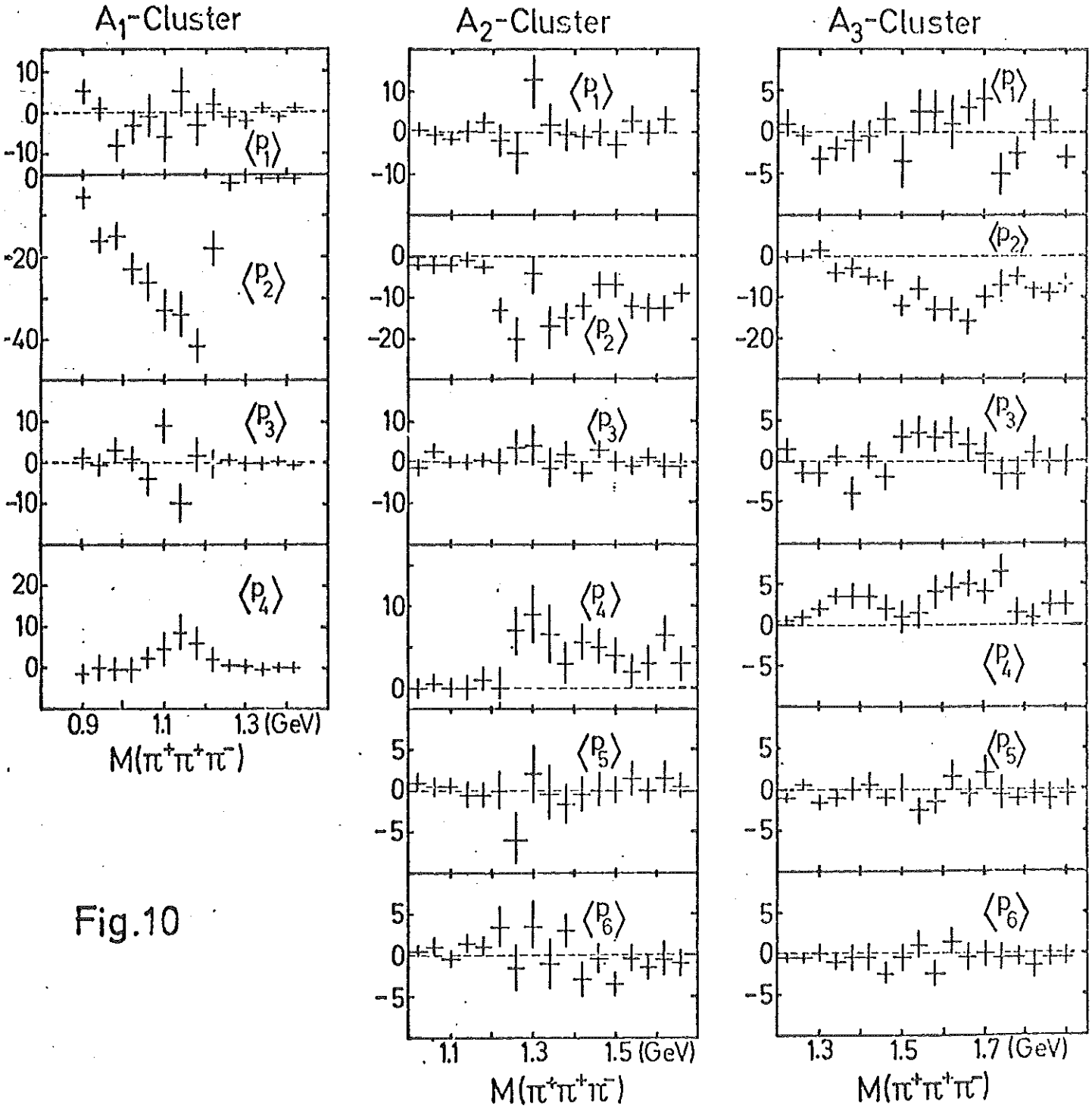
A1-Cluster
A2-Cluster
A3-Cluster
⟨P1⟩
⟨P2⟩
⟨P3⟩
⟨P4⟩
⟨P5⟩
⟨P6⟩
0.9
1.1
1.3 (GeV)
1.3
1.5
1.7 (GeV)
M(π+π+π−)

Fig.10